Article

Effects of Preparation Methods of Pd Supported on (001) Crystal Facets Exposed TiO$_2$ Nanosheets for Toluene Catalytic Combustion

Guiyun Yu [1,*], Chengyan Ge [1,2] and Haiqin Wan [2,*]

1   School of Chemistry and Chemical Engineering, Yancheng Institute of Technology, Yancheng 224000, China
2   Laboratory of Vehicle Emissions Control, School of the Environment, Jiangsu Key Nanjing University, Nanjing 210093, China
*   Correspondence: yuguiyun1@163.com (G.Y.); wanhq@nju.edu.cn (H.W.); Tel.: +86-25-88298280 (G.Y.)

Abstract: A series of TiO$_2$ nanosheets-supported Pd catalysts were individually prepared by impregnation, deposition–precipitation, photo-deposition and in situ reduction by NaBH$_4$. For comparison, Pd supported on P25 was prepared by the impregnation method. The experimental results show that the catalytic efficiency of the catalyst prepared with titanium dioxide nano sheet as the support is higher than that of the catalyst supported with P25. Its excellent properties are as follows: The resulting sample indicates that TiO$_2$ nanosheets-supported Pd catalyst display an improved activity than Pd/P25, whose temperature of 100% complete conversion of toluene decreased by 40 °C at the most. The Pd particles on the catalyst synthesized by the light deposition method and the NaBH$_4$ reduction method are more obvious, while the Pd particles on the catalyst synthesized by the immersion method and the deposition–precipitation method are less obvious, which shows that the latter two methods are more conducive to the dispersion of Pd. The good catalytic activity may be due to the better exposed mirror and dispersion of titanium dioxide nanosheets. This is mainly related to the exposed crystal plane of the nanosheet TiO$_2$ (001), which made it easier to form the oxygen vacancy. Moreover, among all of the TiO$_2$ nanosheets-supported Pd catalysts, Pd/TiO$_2$ NS (TiO$_2$ NS means TiO$_2$ nanosheets) prepared by the impregnation method show the highest catalytic activity. The XRD results show that Pd prepared by impregnation is more dispersed and smaller. This is due to PdO being dispersed more efficiently than the others, leading to more Pd active sites.

Keywords: TiO$_2$ nanosheets; Pd catalyst; prepared method; toluene; catalytic combustion

1. Introduction

Catalytic combustion is a high-efficiency controlling treatment for removing volatile organic compounds (VOCs), and the key issue is to design a suitable catalyst. Considering the crucial role of the support in a catalyst, the interaction between the carrier and the active substance affects its catalytic performance and the oxidation mode of the active species. In particular, these interactions may provide active sites for oxidizing VOCs. For example, CeO$_2$, Nb$_2$O$_5$, La$_2$O$_3$, TiO$_2$, etc., are conducive to the regulation of Pd to PdO [1–4]. Therefore, the form of the carrier and the preparation method of the catalysis are important ways to influence the catalytic performance of the catalyst. The TiO$_2$ material was widely developed and used in the fields of thermal catalysis and photocatalysis owing to its unique properties, certain acid center, adjustable crystal shape and appropriate band gap width [5–9]. The interaction between the metal and the support was observed in TiO$_2$-based catalyst toward the oxidation of the VOCs. Li et al. [10] prepared Ag @ Pd/TiO$_2$ catalyst. Compared with Pd/TiO$_2$, the Pd content (0.2%) was only about one-third of the Pd/TiO$_2$, but showed higher toluene catalytic oxidation activity; T$_{50}$ (T$_{50}$: temperature for 50% conversion) was about 203 °C. Hosseini et al. [11] discussed the role of mesoporous TiO$_2$ in the removal of toluene, and they found that 0.5% Pd-1% Au/TiO$_2$ was an optimal catalyst, T$_{50}$ was 219 °C, and the presence of highly porous structures was a crucial factor.

Additionally, the existence of a strong interaction between TiO_2 and Pd-Au played a vital role in improving the catalytic performance.

The crystal structure and exposed crystal facets of the support are the most important structural parameters affecting the metal–support interaction and its photocatalytic performance [12]. Sun et al. constructed the Pt-TiO_2 film with exposed {0 0 1} facets and showed profoundly higher UV-light-driven photocatalytic activity and stability than that of pure TiO_2 film with exposed {001} facets due to the synergistic effects of exposed {0 0 1} facets and the interaction between the two components [13]. Liu et al. [14] investigated the crystal-plane effect on the CO oxidation properties over the Au/TiO_2 catalyst, showing the order of the catalytic activities as follows: Au/TiO_2−{100} > Au/TiO_2−{101} > Au/TiO_2−{001}. Chen et al. [15] studied the morphology effect of an Au-TiO_2 sample for C_3H_6 epoxidation with H_2 and O_2. There were strong interactions between Au nanoparticles and TiO_2 supporters. The $Au^{\delta-}$ and $Au^{\delta+}$ species exhibited the largest amount of Au/TiO_2{0 0 1} and Au/TiO_2{100}, respectively, leading to different catalytic activity and selectivity. It demonstrated that morphological engineering could act as an effective approach to optimize the catalytic performance and thus deeply understand the catalytic mechanism of oxides. The {101} crystal surface of anatase TiO_2 is the most stable in thermodynamics, while the {001} crystal surface is the most active.

Since 2008, when anatase TiO_2 dominated by a crystal surface of {001} was prepared by Yang et al., much attention has been focused on it, including morphology control, stable exposure of {001} crystal plane by HF and its application [16,17]. In addition to its highly photocatalytic performance [18–20], Deng et al. [21] also found that TiO_2 NS dominated by the {001} crystal surface had higher catalytic properties than TiO_2 nanoparticles in the NH_3-SCR reaction for the catalyst MnO_x/TiO_2.

Therefore, a simple oxide with a clear crystal plane exposure as support is very useful for understanding the metal–support interaction.

In addition, three impregnation methods, including wet impregnation, stepwise impregnation and co-impregnation, were widely used to construct M/TiO_2 samples, and wet impregnation attracted increasing attention in the view of practical operation. For example, Araya et al. adopted the co-impregnation method to investigate the effect of different supports (Al_2O_3, ZrO_2 and SiO_2) [22]. Yuan et al. prepared a series of Pt/TiO_2 catalysts using $NaBH_4$ as a reduction agent. The effects of loading amount of Pt and exposed crystal planes of TiO_2 on the physical and chemical properties, and the catalytic performance in HCHO oxidation reaction were investigated [16]. The status of the metal component is related to the preparation methods. The surface configuration of as-synthesized catalysts could be regulated by various synthesis parameters, such as heating temperature, deposition amount, loading method or the impregnation order [23–25]. Su et al. revealed that the catalytic performance of NO reduction over Fe-Ag/Al_2O_3, including its selectivity and catalytic activity, was affected by the preparation method [26]. Furthermore, our group successfully synthesized CuO-CeO_2/γ-Al_2O_3 and FeOx-CeO_2/γ-Al_2O_3 catalysts, indicating that the impregnation order determined their dispersion state and catalytic activity [23,27].

The Pd-based catalysts are a common catalyst for VOCs' combustion. The status of Pd and the metal–support interaction are two key issues for exploring the catalytic mechanism. In this study, Pd/TiO_2 NS was selected as the model catalyst to study the effect of the preparation method on the catalytic activity of toluene. The metal–support interaction was investigated by tuning the prepared methods to obtain different Pd species. The main focuses were: (1) $Ti(OC_4H_9)_4$ was used as the titanium source and HF as the etching agent to synthesize TiO_2 nanosheets exposed {001} by the hydrothermal method; (2) TiO_2 NS was used as the support to prepare the Pd/TiO_2 NS catalyst different ways (the impregnation method, the deposition–precipitation method, the photo-deposition method, the $NaBH_4$ reduction method), and the influence of the preparation method on the catalytic activity of toluene was studied; (3) The metal–support interaction of these catalysts was analyzed by the characterization techniques of BET, TEM, XRD, XPS and H_2-TPR.

2. Results and Discussion

2.1. Catalytic Performance of Toluene Oxidation

The light-off curves of the catalytic combustion of toluene over the Pd/TiO$_2$ catalysts are shown in Figure 1. Two results are observable in the figure. Firstly, the catalyst prepared by the immersion method had the highest catalytic activity when the temperature ranged from 170 to 210 °C. The temperature of the toluene complete conversion decreased by 40 °C at most (from 250 °C by Pd/TiO$_2$ P25-IM to 210 °C by Pd/TiO$_2$ NS-IM). This was due to the unique property of TiO$_2$ NS. Some similar results were previously reported [28,29]. Secondly, the light-off curves of Pd/TiO$_2$ NS were complicated. Among these results, Pd/TiO$_2$ NS-IM showed the highest catalytic performance; 100% conversion of toluene was achieved at 210 °C. For Pd/TiO$_2$ NS-DP and Pd/TiO$_2$ NS-PD, their light-off curves were similar with that of Pd/TiO$_2$ P25 before 210 °C, and Pd/TiO$_2$ NS-DP reached 100% conversion at 230 °C while Pd/TiO$_2$ NS-PD and Pd/TiO$_2$ P25 were reached at 250 °C. For Pd/TiO$_2$ NS-NaBH$_4$, its activity was higher than Pd/TiO$_2$-NS-DP before 210 °C, but its catalytic rate decreased thereafter and it reached the toluene 100% conversion at 270 °C. This result indicated that the status and metal–support interaction of Pd are different on each Pd/TiO$_2$ NS catalyst, which was related to its catalytic performance. To understand the detailed reasons, the physicochemical properties of these Pd/TiO$_2$ NS catalysts were analyzed.
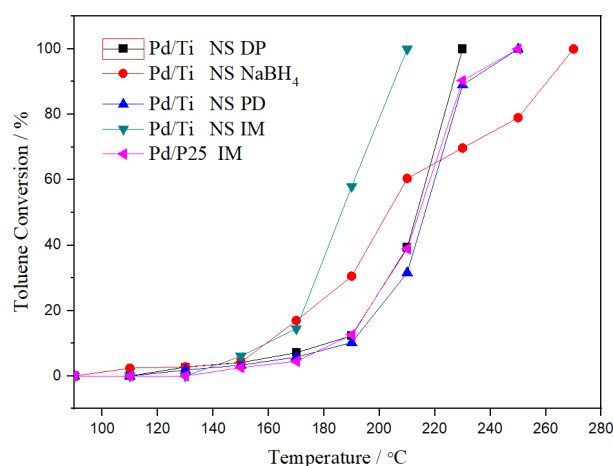

Figure 1. Catalytic oxidation of toluene by Pd/TiO$_2$ catalyst prepared by different methods.

2.2. BET and TEM Analysis

As displayed in Table 1, the specific surface area values of Pd/TiO$_2$ catalysts prepared by the deposition–precipitation, photo-deposition, NaBH$_4$ reduction and impregnation methods are 80 m^2/g, 77 m^2/g, 74 m^2/g and 52 m^2/g, respectively, which are all lower than that of TiO$_2$ nanometer sheets (92 m^2/g). At the same time, we also provided the pore size and pore volume of the samples, which should be stacking holes. It was observed that the pore volume of the catalyst decreased after Pd loading. The large specific surface area of the catalysts provided more active sites, resulting in the enhanced catalytic activity over TiO$_2$ NS as compared with P25. After Pd loading onto TiO$_2$ NS, the specific surface area values of all Pd/TiO$_2$ catalysts were decreased with the lowest value for the Pd/TiO$_2$ NS-IM sample due to its well-dispersion of Pd nanoparticles onto the TiO$_2$ NS surface [30]. This was further demonstrated by the following TEM data, which may be one of the reasons for its improved activity.

Figure 2 shows the HRTEM and TEM images of the synthesized TiO$_2$ nanometer sheet. From Figure 2a, the d spacing was 0.35 nm and 0.47 nm, corresponding to (101) and (002) of anatase TiO$_2$, respectively, which were in line with the previous report [31]. As shown in Figure 2c,d, TiO$_2$ (NS) clearly showed a uniform flake shape, with an average length of about 50 nm and an average thickness of about 7 nm. The TEM images of the Pd/TiO$_2$ NS (Figure 3) catalysts prepared by the different methods, among which Figure 3a–d

were the catalysts synthesized by photo-deposition, $NaBH_4$ reduction, impregnation and deposition–precipitation, respectively. By comparing both Figures 2 and 3, it can be easily seen that the flake shape of TiO_2 NS was retained after the Pd was supported by any of the prepared methods, indicating that the structure of TiO_2 NS was stable when prepared by HF etching. This is consistent with the literature [32]. Furthermore, the sizes of Pd particles were different from each other. The Pd particles were clearly observed in Pd/TiO_2 NS-PD and Pd/TiO_2 NS-DP. For the other catalysts, some ultrafine Pd particles were observed as marked by red circles. However, for Pd/TiO_2 NS-IM it was difficult to find them on the TiO_2 support (Figure 3c). In consideration of the highest catalytic activity over Pd/TiO_2 NS-IM, the results indicated that the Pd species were highly dispersed on the TiO_2 NS surface in Pd/TiO_2 NS-IM. Combined with the TEM result in Figure 3, we can reasonably infer that the particle sizes of Pd are increased in the order of Pd/TiO_2 NS-IM < Pd/TiO_2 NS-$NaBH_4$ < Pd/TiO_2 NS-DP < Pd/TiO_2 NS-PD. The reduction order of particle size was consistent with their specific surface areas for the catalysts, which further demonstrated that the Pd nanoparticles were deposited onto the supporter. The highest dispersion degree and smallest size of the Pd nanoparticles onto the Pd/TiO_2 NS-IM surface resulted in excellent catalytic activity [30].

Table 1. The physical properties of the samples.

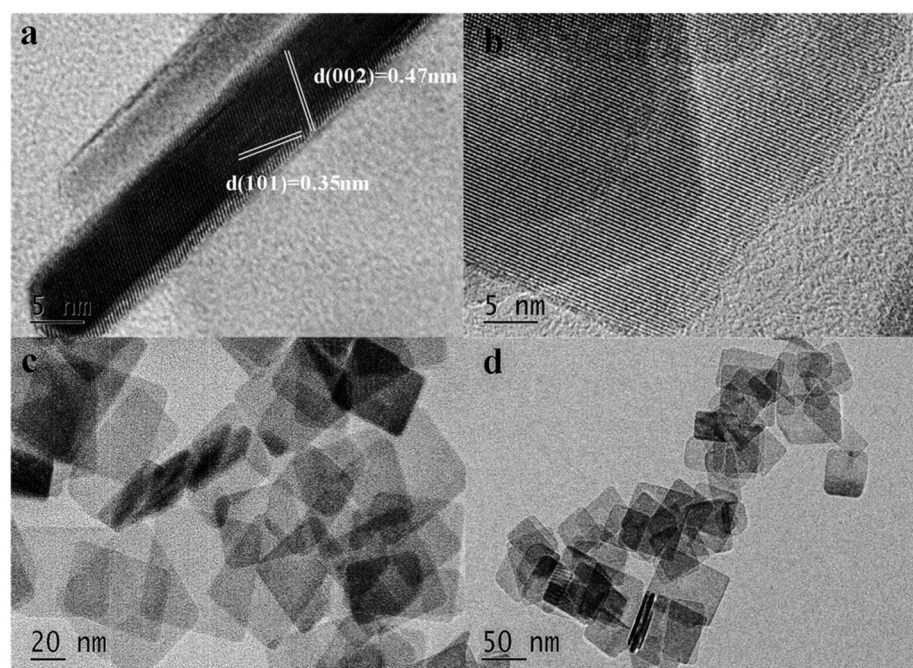| Catalyst	Surface Area m^2/g	Pore Volume cm^3/g	Pore Size nm
P25	50	0.4	21
TiO_2 NS	92	0.43	18.1
Pd/TiO_2 NS-DP	80	0.38	20.1
Pd/TiO_2 NS-PD	77	0.38	17.9
Pd/TiO_2 NS-$NaBH_4$	74	0.37	20.1
Pd/TiO_2 NS-IM	52	0.22	25.2

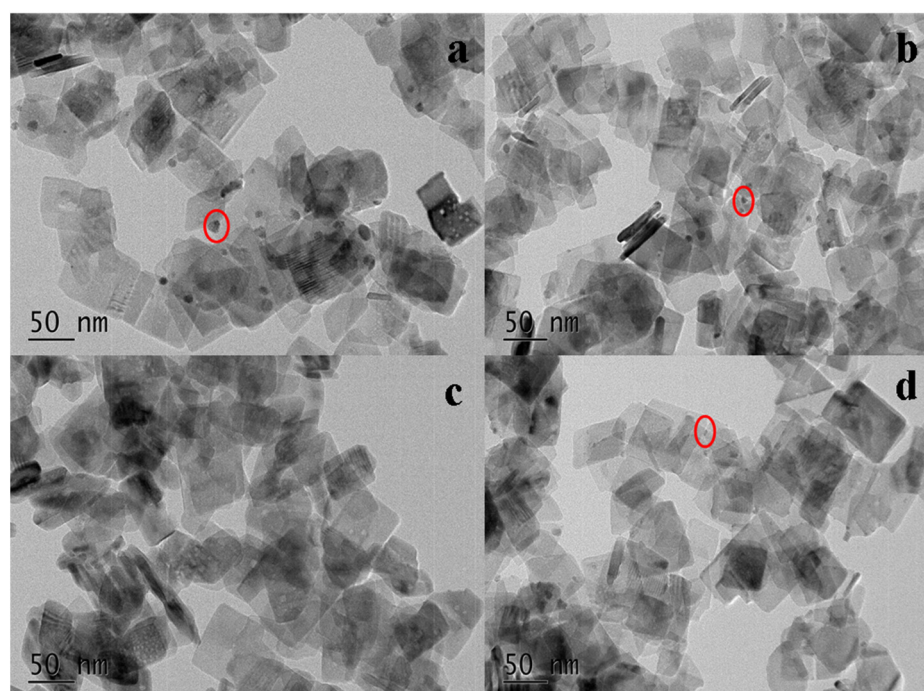**Figure 2.** HRTEM (**a,b**) and TEM (**c,d**) diagrams of TiO_2(NS).

Figure 3. TEM image of Pd/TiO$_2$ catalyst prepared by different methods: (**a**) the photo-deposition method; (**b**) the deposition–precipitation method; (**c**) the impregnation method; (**d**) the NaBH$_4$ reduction method.

2.3. XRD Analysis

Figure 4 shows the characteristic X-ray diffraction peaks of TiO$_2$ (NS), P25 and Pd/TiO$_2$ (NS) samples prepared by various methods. Among the results were some characteristic diffraction peaks of rutile TiO$_2$ besides anatase TiO$_2$ in the P25 samples (JCPSD-89-4920) [33], while there were characteristic diffraction peaks of anatase TiO$_2$ in all TiO$_2$ NS-based samples (JCPDS-21-1272) [20]. The observed diffraction peak {004} (and diffraction peak {200} on TiO$_2$ NS as marked by red arrows were somewhat narrow compared with P25, which may be due to the anisotropic growth of the crystal along the direction of {100}, which was consistent with the results observed by Deng et al. [21]. In addition, the Pd/TiO$_2$ catalysts prepared by different methods (the impregnation method, the deposition–precipitation method, the photo-deposition method, the NaBH$_4$ reduction method) showed the consistency between anatase peak of TiO$_2$ and TiO$_2$ nanocrystalline sheets, indicating that these preparation methods did not change the crystal structure of the TiO$_2$ nanocrystalline sheets. We did not find the characteristic diffraction peak of Pd in the XRD patterns, which may be due to the efficient dispersion of Pd or because the load was lower than the detection limit.

2.4. H$_2$-TPR Analysis

Figure 5 shows the H$_2$-TPR diagram of catalysts Pd/TiO$_2$ NS. As shown in the figure, the reduction peaks below 100 °C were attributed to the reduction peaks of Pd species [34]. All of the Pd/TiO$_2$ NS samples showed a reduction peak of Pd species at around 75 °C, while Pd/ P25 showed this peak at 84 °C [35]. Huan Chen et al. obtained similar results [36]. This is mainly due to nanosheet TiO$_2$ having a more {001} exposed crystal surface, which is easy to reduce [37]. E. López et al. [38] developed a Pd/Al$_2$O$_3$ sample for the catalytic hydrodechlorination of chlorobenzene, exhibiting that the loading amount and size of the Pd nanoparticles onto the Al$_2$O$_3$ surface directly determined their catalytic performance. A strong metal–support interaction existed through the deposition of Pd metal nanoparticles with a small size, owing to its intrinsic size effect [34], while Pd particles with a large size were beneficial to the formation of β-PdH [39,40]. Notably, for all samples, the characteristic

H_2 consumption peaks imply that PdO species onto the TiO_2 NS surface benefits the H_2 reduction even below room temperature. Additionally, the supported Pd nanoparticles were susceptible to activating and storing H_2, which is more conducive to improving the catalytic activity of p-toluene oxidation under mild ambient conditions. In the hydrogen atmosphere, more oxygen vacancy will be generated on the surface of Pd/TiO_2 NS, which is conducive to improving the catalytic activity of p-toluene oxidation.
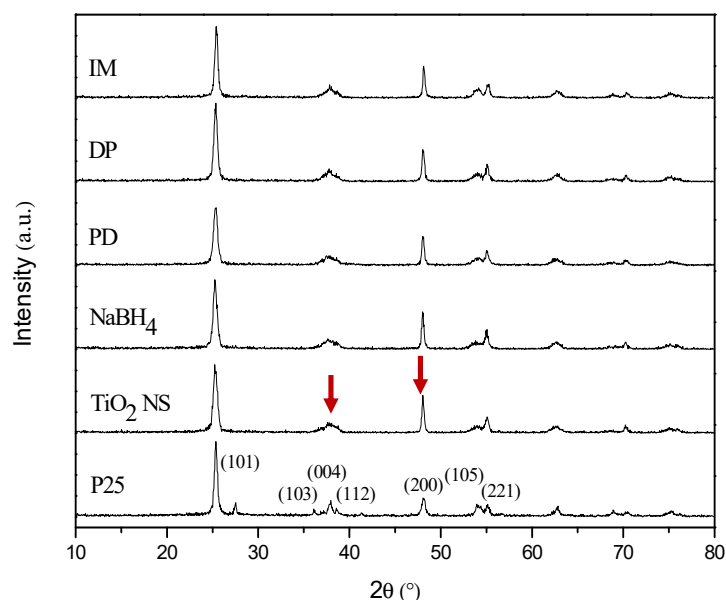

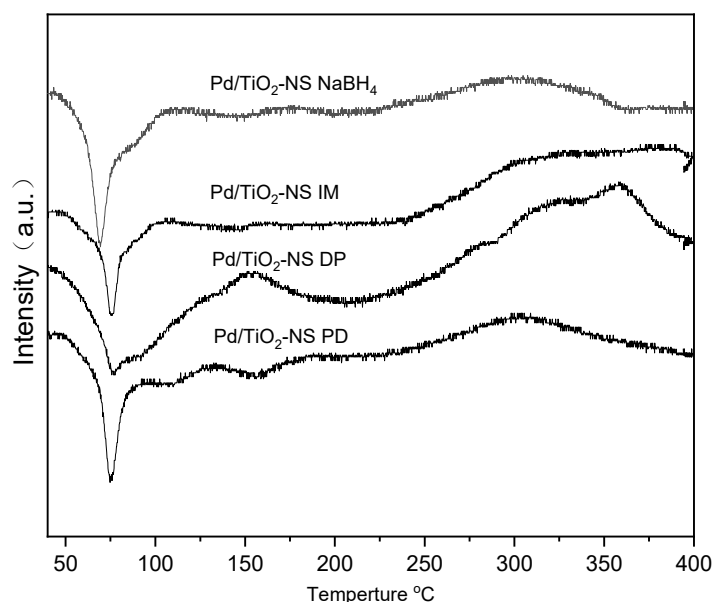**Figure 4.** XRD patterns of Pd/TiO_2 prepared by different methods.

Figure 5. H_2-TPR diagram of the catalyst prepared by different preparation methods.

2.5. XPS Analysis

To investigate elemental compositions and chemical states, the XPS spectra of Pd/TiO_2 NS-IM, Pd/TiO_2 NS-DP, Pd/TiO_2 NS-NaBH$_4$ and Pd/TiO_2 NS-PD are exhibited in Figure 6 [41–43]. Two signals at 336.4 eV and 341.6 eV corresponded to Pd 3d$_{5/2}$ and Pd 3d$_{3/2}$, respectively, indicating their chemical state of Pd^{2+} in the Pd/TiO_2 samples. This result is similar to the reported Pd/Al_2O_3 catalyst prepared by the impregnation method [44,45]. Similar to the Pd/TiO_2 NS sample, the binding energies of Pd/Al_2O_3 and Pd/SiO_2 are shifted to the

lower energy due to the formation of low valence Pd^0 species [46], which may be caused by a reductive environment. It also shows that the interaction is strong between the active substance of the catalyst and the support. The strong interaction between Pd nanoparticles could result in the deficiency of the electron of Pd in Pd/TiO_2 NS, which may enable more toluene molecules to be adsorbed on the catalyst surface and improve the catalytic activity. This is consistent with our previous results [47].
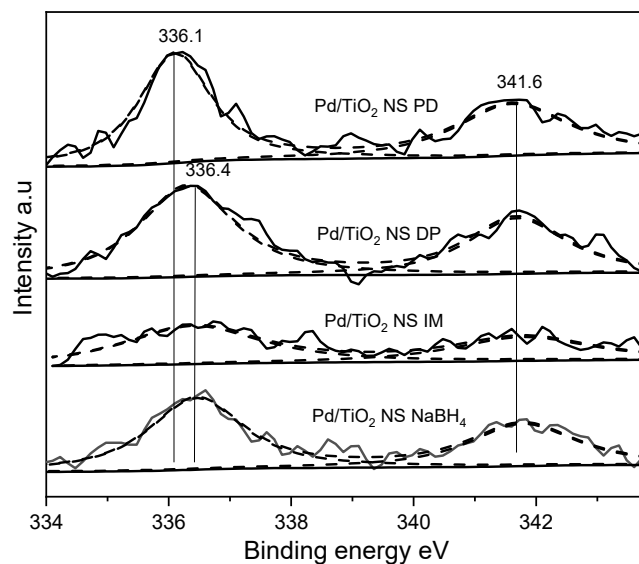

Figure 6. Pd 3d XPS spectra of different catalysts.

3. Materials and Methods

3.1. Catalyst Preparation

Preparation of TiO$_2$ Nanosheets (TiO$_2$ NS)

A total of 20 mL $Ti(OC_4H_9)_4$ was mixed with 3.2 mL of HF solution (50 wt.%) at room temperature, and then transferred to a 100 mL Teflon-lined autoclave for subsequent heating at 200 °C for 24 h. The obtained powder was collected and washed alternately with ethanol and distilled water more than 6 times to remove the remaining fluorine. The TiO_2 NS was achieved by drying at 110 °C for 24 h.

Preparation of the Pd/TiO$_2$ NS and Pd/P25 Catalysts

The impregnation method: A total of 1 g TiO_2 NS powder was first added to the $PdCl_2$ solution, and then heated at 80 °C and constantly stirred until the water was fully removed. The obtained sample was dried in an oven at 110°C for 12 h, and then ground and calcined at 400 °C for 4 h. The resulting catalyst was denoted as Pd/TiO_2 NS-IM. To obtain the Pd/P25-IM catalyst, the previous steps were followed and TiO_2 NS was replaced with P25.

The deposition–precipitation method: The $PdCl_2$ solution was mixed with TiO_2 NS powder, continuously stirred and pH was adjusted with 1 mol/L Na_2CO_3 to pH = 10.5. The mixed solution was stirred under magnetic power for 2 h. The material obtained was washed with distilled water until the pH value reached neutral, and then dried at 110 °C overnight. Finally, the obtained powder was calcined at 400 °C for 4 h. The resulting sample was Pd/TiO_2 NS-DP.

The $NaBH_4$ reduction method: The mixed solution of PVP and $PdCl_2$ (Pd/PVP quality ratio = 1.0:1.5) was placed in the ice bath and stirred for 20 min before adding $NaBH_4$ solution (Pd/$NaBH_4$ mole ratio = 1.0:5.0). TiO_2 NS powder was then dispersed in the above-mentioned mixture and stirred for 6 h. The solid obtained by filtration and cleaning was dried at 80 °C. Finally, the powder was calcined at 400 °C for 4 h and then collected as Pd/TiO_2 NS-$NaBH_4$.

The photo-deposition method: The mixture of TiO_2 NS powder and $PdCl_2$ solution was placed in the reactor in darkness and the ice bath and stirred for 20 min after adding 5 mL of methanol. The mixture was constantly stirred and nitrogen was pumped into it with a flow rate of 60 mL/min for 1 h. The mixture was placed under a 500 W high pressure UV mercury lamp and continuously illuminated for 4 h. The material obtained was washed with distilled water, dried at 110 °C and then ground powder was calcined at 400 °C for 4 h. The catalyst obtained was denoted as Pd/TiO_2 NS-PD.

The mass proportion of the metal element Pd in all of the catalysts was 1%.

3.2. Catalyst Characterization

The X–ray diffraction (XRD) was performed on a Philips X'pert Pro diffraction meter using Cu Kα radiation (λ = 1.5408 Å) at 40 kV and 40 mA at room temperature. These data were collected at the scan rate of 5° min^{-1} between 10–80° (2q). The Brunauer–Emmett–Teller (BET) surface area determination and Barret–Joyner–Halenda (BJH) pore volume and size analysis were measured on an ASAP 2020 instrument at 77 K according to the N_2 adsorption–desorption isotherms. Transmission electron microscopic (TEM) and higher-resolution transmission electron microscopy (HRTEM) images were collected by using a JEM-200CX at an acceleration voltage of 200 kV.

The binding energies of Pd of the synthetic material were measured by an X-ray photoelectron spectra (XPS), which was carried out by an ESCALAB250Xi photoelectron spectrometer with a monochromatic Al Kα source (hv = 1486.6 eV) and a charge neutralizer. The hydrogen temperature programmed reduction (H2-TPR) experiment was conducted on the Finesorb-3010 instrument, which was equipped with a thermal conductivity detector (TCD). During the experiment, 100 mg of the sample was first put into a quartz tube, preheated at 110 °C for 1 h under N2 atmosphere, and then cooled to room temperature. Then, a 10% H_2/Ar gas mixture (50 mL min^{-1}) was introduced into the sample tube and the sample was heated to 200 °C at the heating rate of 10 °C·min^{-1}.

3.3. Catalytic Performance Test

Oxidation of toluene was conducted in a continuous down-flow fixed-bed micro reactor under atmospheric pressure. Briefly, a 100 mg sample (pressed and sieved through 40–60 mesh) was pretreated in a H2 stream (40 mL min^{-1}) at 300 °C for 2 h, then cooled to 100 °C. Subsequently, the toluene with a constant-flow pump at a rate of 0.0104 mL h^{-1} was delivered into a mixed-flow gas, which contained 30% oxygen, 70% nitrogen, with a total flow of 40 mL min^{-1}, for a space velocity of 24,000 mL gcat^{-1} h^{-1}. The products were analyzed online by a gas chromatograph equipped with a Porapak Q-packed column and a thermal conductivity detector (TCD). To obtain accurate results, each experiment was performed three times in parallel with a sustained reaction duration of no less than 30 min. The average value was used as the activity at each temperature.

4. Conclusions

Although nano TiO_2 have been widely used as photocatalysts and obtained good activity effects, their application is still limited by the short life of the photoexcited charge carriers and the wide band gap requiring ultraviolet (UV) radiation. In this study, the TiO_2 NS was used as Pd-based carrier to prepare the Pd/TiO_2 NS catalyst, which was applied to study the catalytic combustion performance of VOCs and was found to have very good catalytic activity.

Firstly, TiO_2 nanocrystalline was synthesized by the hydrothermal synthesis method with HF as the etching agent, and then the single metal Pd/TiO_2 NS catalyst was synthesized by different methods (the impregnation method, the deposition–precipitation method, the photo-deposition method and the $NaBH_4$ reduction method). The relationship between the catalyst structure and the catalytic combustion activity of toluene was studied by combining with BET, TEM, XRD, H_2-TPR and other characterization techniques. In the future, we will be committed to improving the reaction mechanism of TiO_2 NS-supported

Pd catalysts for VOCs' combustion, reducing TiO_2 NS support to form defects on its surface and reloading Pd and studying the effect of surface defects on catalyst performance. The conclusions obtained in this work are as follows:

(1) Pd/TiO_2 catalysts were synthesized by different methods to study the effects of different preparation methods on the catalytic combustion activity of toluene. Firstly, we compared the catalytic activity of toluene with that of ordinary commercial P25 and TiO_2 nanometer tablets after impregnating the Pd. The results showed that Pd/TiO_2 NS with {001} crystal surface as the exposed crystal surface was significantly better than Pd/P25, and the temperature of 100% complete transformation of toluene was 40 °C lower. This is mainly because the {001} crystal surface of nano-sheet TiO_2 is easier to form oxygen vacancy;

(2) According to the experimental results, the catalyst prepared by the impregnation method had smaller Pd particles and more active sites. The smaller the Pd particles, the better the catalytic performance. The 100% conversion of toluene was achieved at 210 °C on Pd/ TiO_2-IM. The catalytic activity of Pd / TiO_2 catalyst prepared by the illumination (Pd/TiO_2-PD) and deposition–precipitation (Pd/ TiO_2-DP) methods was lower than that of Pd / TiO_2 catalyst prepared by immersion method. Compared with the other synthesis methods, Pd in the impregnation method may be dispersed better in the synthesis process and the particles are smaller, so that more Pd active sites can be spread on the TiO_2 nano-sheet carrier.

Author Contributions: Conceptualization, H.W.; Formal analysis, G.Y. and C.G.; Investigation, G.Y. and C.G.; Methodology, G.Y., and C.G.; Project administration, H.W.; Writing—original draft, G.Y., and C.G.; Writing—review & editing, G.Y., C.G. and H.W.; All authors have read and agreed to the published version of the manuscript.

Data Availability Statement: Not applicable.

Conflicts of Interest: The authors declare no conflict of interest.

References

1. Fujimoto, T.M.; Ponczek, M.; Rochetto, U.L.; Tomaz, E. Photocatalytic oxidation of selected gas-phase VOCs using UV light, TiO_2, and TiO_2/Pd. *Environ. Sci. Pollut. Res.* **2017**, *24*, 6390–6396. [CrossRef] [PubMed]
2. Lin, H.-Q.; Chen, Y.W. Complete oxidation of toluene on Pd/modified-CeO_2 catalysts. *J. Taiwan Inst. Chem. Eng.* **2016**, *67*, 69–73. [CrossRef]
3. Shao, Y.; Xia, Q.; Liu, X.; Lu, G.; Wang, Y. $Pd/Nb_2O_5/SiO_2$ catalyst for the direct hydrodeoxygenation of biomass-related compounds to liquid alkanes under mild conditions. *ChemSusChem* **2015**, *8*, 1761–1767. [CrossRef]
4. Zhou, Y.; Lu, H.F.; Zhang, H.H.; Chen, Y.F. Catalytic properties of $LaBO_3$ perovskite catalysts in VOCs combustion. *China Environ. Sci.* **2012**, *32*, 1772–1777.
5. Zhang, C.; Hong, H.; Tanaka, K.I. Catalytic performance and mechanism of a Pt/TiO_2 catalyst for the oxidation of formaldehyde at room temperature. *Appl. Catal. B Environ.* **2006**, *65*, 37–43. [CrossRef]
6. Liu, C.; Zhang, Q.; Hou, W.; Zou, Z. Two-dimensional titanium/niobium metal oxide-based materials for photocatalytic application. *Sol. RRL* **2020**, *4*, 2000070. [CrossRef]
7. Liu, C.; Sun, T.; Wu, L.; Liang, J.; Huang, Q.; Chen, J.; Hou, W. N-doped $Na_2Ti_6O_{13}$@TiO_2 core-shell nanobelts with exposed {1 0 1} anatase facets and enhanced visible light photocatalytic performance. *Appl. Catal. B Environ.* **2015**, *170*, 17–24. [CrossRef]
8. Zhang, Z.; Chen, M.; Shangguan, W. Low-temperature SCR of NO with propylene in excess oxygen over the Pt/TiO_2 catalyst. *Catal. Commun.* **2009**, *10*, 1330–1333. [CrossRef]
9. Zhang, Z.X.; Chen, M.X.; Jiang, Z.; Shangguan, W.F. Performance and mechanism study for low-temperature SCR of NO with propylene in excess oxygen over Pt/TiO_2 catalyst. *J. Environ. Sci.* **2010**, *22*, 1441–1446. [CrossRef]
10. Li, Y.; Liu, F.; Fan, Y.; Cheng, G.; Song, W.; Zhou, J. Silver palladium bimetallic core-shell structure catalyst supported on TiO_2 for toluene oxidation. *Appl. Surf. Sci.* **2018**, *462*, 207–212. [CrossRef]
11. Hosseini, M.; Siffert, S.; Tidahy, H.L.; Cousin, R.; Lamonier, J.F.; Aboukais, A.; Vantomme, A.; Roussel, M.; Su, B.L. Promotional effect of gold added to palladium supported on a new mesoporous TiO_2 for total oxidation of volatile organic compounds. *Catal. Today* **2007**, *122*, 391–396. [CrossRef]

12. Liu, C.; Zhang, Q.; Zou, Z. Recent advances in designing ZnIn₂S₄-based heterostructured photocatalysts for hydrogen evolution. *J. Mater. Sci. Technol.* **2023**, *139*, 167–188. [CrossRef]

13. Sun, J.; Zhang, M.; Wang, Z.F.; Chen, H.Y.; Chen, Y.; Murakami, N.; Ohno, T. Synthesis of anatase TiO₂ with exposed {001} and {101} facets and photocatalytic activity. *Rare Met.* **2019**, *4*, 287–291. [CrossRef]

14. Liu, L.C.; Gu, X.R.; Ji, Z.Y. Crystal-Plane Effects on the Catalytic Properties of Au/TiO₂. *ACS Catal.* **2013**, *3*, 2768–2775. [CrossRef]

15. Chen, S.; Zhang, B.; Su, D.; Huang, W. Titania Morphology-Dependent Gold–Titania Interaction, Structure, and Catalytic Performance of Gold/Titania Catalysts. *Chemcatchem* **2015**, *7*, 3290–3298. [CrossRef]

16. Zeng, Y.; Jiang, L.; Zhang, X.; Xie, S.; Pei, Y.; Zhou, G.; Hua, W.; Qiao, M.; Li, Z.H.; Zong, B. Effect of Titania Polymorphs on the Structure and Catalytic Performance of the Pt-WOx/TiO2 Catalyst in Glycerol Hydrogenolysis to 1,3-Propanediol. *ACS Sustain. Chem. Eng.* **2022**, *10*, 9532–9545. [CrossRef]

17. Su, Y.; Ji, K.; Xun, J.; Zhang, K.; Liu, P.; Zhao, L. Catalytic oxidation of low concentration formaldehyde over Pt/TiO₂ catalyst. *Chin. J. Chem. Eng.* **2021**, *29*, 190–195. [CrossRef]

18. Feng, L.; Zheng PFu, Y.L. Pt/TiO₂ Nanosheets Array Dominated by {001} Facets with Enhanced Photocatalytic Activity. *Chin. J. Chem. Phys.* **2014**, *27*, 530–534.

19. Gao, Z.; Cui, Z.; Zhu, S.; Liang, Y.; Li, Z.; Yang, X. Fabrication, characterization, and photocatalytic properties of anatase TiO₂ nanoplates with exposed {001} facets. *J. Nanopart Res.* **2014**, *16*, 2191. [CrossRef]

20. Tang, K.; Wang, Z.; Zou, W.; Guo, H.; Wu, Y.; Pu, Y.; Tong, Q.; Wan, H.; Gu, X.; Dong, L.; et al. Advantageous Role of Ir0 Supported on TiO₂ Nanosheets in Photocatalytic CO₂ Reduction to CH₄: Fast Electron Transfer and Rich Surface Hydroxyl Groups. *ACS Appl. Mater. Interfaces* **2021**, *13*, 6219–6228. [CrossRef]

21. Deng, S.C.; Fan, Y.Y.; Meng, T.T.; Gao, B.L.; Ding, F. Advanced MnOx/TiO₂ Catalyst with Preferentially Exposed Anatase {001} Facet for Low-temperature SCR of NO. *ACS Catal.* **2016**, *6*, 5807–5815. [CrossRef]

22. Guila, G.; Gracia, F.; Araya, P. CuO and CeO₂ catalysts supported on Al₂O₃, ZrO₂, and SiO₂ in the oxidation of CO at low temperature. *Appl. Catal. A Gen.* **2008**, *1*, 16–24.

23. Sun, J.; Ge, C.; Yao, X.; Zou, W.; Hong, X.; Tang, C.; Dong, L. Influence of different impregnation modes on the properties of CuO CeO₂/Al₂O₃ catalysts for NO reduction by CO. *Appl. Surf. Sci.* **2017**, *426*, 279–286. [CrossRef]

24. Huang, W.; Zuo, Z.; Han, P.; Li, Z.; Zhao, T. XPS and XRD investigation of Co/Pd/TiO₂ catalysts by different preparation methods. *J. Electron Spectrosc. Relat. Phenom.* **2009**, *173*, 88–95. [CrossRef]

25. Ataloglou, T.; Vakros, J.; Bourikas, K.; Fountzoula, C.; Kordulis, C.; Lycourghiotis, A. Influence of the preparation method on the structure–activity of cobalt oxide catalysts supported on alumina for complete benzene oxidation. *Appl. Catal. B Environ.* **2005**, *57*, 299–312. [CrossRef]

26. Yang, X.; Su, Y.X.; Qian, W.Y.; Yuan, M.H.; Zhou, H.; Deng, W.Y.; Zhao, B.T. Experimental study on selective catalytic reduction of NO by C3H6 over Fe-Ag/Al₂O₃ catalysts. *J. Fuel Chem. Technol.* **2017**, *45*, 1365–1375. [CrossRef]

27. Ge, C.; Yu, Y.; An, D.; Tong, Q.; Tang, C.; Gao, F.; Sun, J.; Dong, L. Surface configuration modulation for FeOx-CeO₂/γ-Al₂O₃ catalysts and its influence in CO oxidation. *J. Catal.* **2020**, *386*, 139–150. [CrossRef]

28. Zhang, Y.; Zeng, H.; Jia, B.; Wang, Z.H.; Liu, Z.M. Selective catalytic reduction of NOx by H₂ over Pd/TiO₂ catalyst. *Chin. J. Catal.* **2019**, *40*, 849–855. [CrossRef]

29. Li, L.; Jiang, F.; Wan, H.; Zheng, S. TiO₂ Nanosheet: Synthesis and Photocatalytic Performance for Phenol Degradation. *Chin. J. Inorg. Cheemistry* **2011**, *27*, 1041–1046.

30. Denkwitz, Y.; Makosch, M.; Geserick, J.; Hörmann, U.; Selve, S.; Kaiser, U.; Hüsing, N.; Behm, R.J. Influence of the crystalline phase and surface area of the TiO₂ support on the CO oxidation activity of mesoporous Au/TiO₂ catalysts. *Appl. Catal. B Environ.* **2009**, *91*, 470–480. [CrossRef]

31. Xiao, H.Y.; Zhen, L.; Sun, C.; Hua, G.Y.; Li, C. Hydrothermal Stability of {001} Faceted Anatase TiO₂. *Chem. Mater.* **2011**, *23*, 3486–3494.

32. Shi, T.; Duan, Y.; Lv, K.; Hu, Z.; Li, Q.; Li, M.; Li, X. Photocatalytic Oxidation of Acetone Over High Thermally Stable TiO₂ Nanosheets With Exposed (001) Facets. *Front. Chem.* **2018**, *6*, 175–178. [CrossRef] [PubMed]

33. Di, L.; Li, Z.; Lee, B.; Park, D.W. An alternative atmospheric-pressure cold plasma method for synthesizing Pd/P25 catalysts with the assistance of ethanol. *Int. J. Hydrog. Energy* **2017**, *42*, 11372–11378. [CrossRef]

34. Komhom, S.; Mekasuwandumrong, O.; Praserthdam, P.; Panpranot, J. Improvement of Pd/Al₂O₃ catalyst performance in selective acetylene hydrogenation using mixed phases Al₂O₃ support. *Catal. Commun.* **2008**, *10*, 86–91. [CrossRef]

35. Zhao, B. Characterization of Pd Catalysts by Temperature Programmed Reduction and Temperature Programmed Desorption. *Precious Met.* **2011**, *32*, 1–3.

36. Chen, H.; Shao, Y.; Xu, Z.; Wan, H.; Wan, Y.; Zheng, S.; Zhu, D. Effective catalytic reduction of Cr(VI) over TiO₂ nanotube supported Pd catalysts. *Appl. Catal. B Environ.* **2011**, *105*, 255–262. [CrossRef]

37. He, Z.; Wen, L.; Wang, D.; Xue, Y.; Lu, Q.; Wu, C.; Chen, J.; Song, S. Photocatalytic Reduction of CO₂ in Aqueous Solution on Surface-Fluorinated Anatase TiO₂ Nanosheets with Exposed {001} Facets. *Energy Fuels* **2014**, *28*, 3982–3993. [CrossRef]

38. Lpez, E.; Ordfiez, S.; Diez, F.V.; Sastre, H. Hydrodechlorination of chlorobenzene tetrachloroethylene mixtures over a Pd/Al₂O₃ csatalyst. *Stud. Surf. Sci. Catal.* **2001**, *133*, 521–526.

39. Fagherazzi, G.; Benedetti, A.; Polizzi, S.; Mario, A.; Pinna, F.; Signoretto, M.; Pernicone, N. Structural investigation on the stoichiometry of β-PdHxin Pd/SiO$_2$ catalysts as a function of metal dispersion. *React. Kinet. Catal. Lett.* **1995**, *32*, 293–303. [CrossRef]

40. Pinna, F.; Signoretto, M.; Strukul, G.; Polizzi, S.; Pernicone, N. Pd-SiO$_2$ catalysts. stability of β-PdHxas a function of Pd dispersion. *React. Kinet. CataI. Lett.* **1997**, *60*, 9–13. [CrossRef]

41. Liu, C.; Zhang, Y.; Wu, J.; Dai, H.; Ma, C.; Zhang, Q.; Zou, Z. Ag-Pd alloy decorated ZnIn$_2$S$_4$ microspheres with optimal Schottky barrier height for boosting visible-light-driven hydrogen evolution. *J. Mater. Sci. Technol.* **2022**, *114*, 81–89. [CrossRef]

42. Liu, C.; Han, Z.; Feng, Y.; Dai, H.; Zhao, Y.; Han, N.; Zhang, Q.; Zou, Z. Ultrathin direct Z-scheme 2D/2D N-doped HTiNbO5 nanosheets/g-C3N4 porous composites for efficient photocatalytic degradation and H2 generation under visible light. *J. Colloid Interface Sci.* **2021**, *583*, 58–70. [CrossRef] [PubMed]

43. Liu, C.; Feng, Y.; Han, Z.; Sun, Y.; Wang, X.; Zhang, Q.; Zou, Z. Z-scheme N-doped K$_4$Nb$_6$O$_{17}$/g-C$_3$N$_4$ heterojunction with superior visible-light-driven photocatalytic activity for organic pollutant removal and hydrogen production. *Chin. J. Catal.* **2021**, *42*, 164–174. [CrossRef]

44. Wu, Q.; Gao, Z.; He, F.; Xu, G. XPS study on the deactivated Pdd Pde$_2$O$_3$ catalyst for CO coupling reaction with ammonia. *J. Tianjin Inst. Technol.* **2003**, *19*, 24–27.

45. Gao, Z.; Li, H.; Xu, J.; Zeng, Y. XPS analysis and gas sensing properties of Pd doped SnO$_2$ films. *Electron. Compon. Mater.* **2011**, *30*, 27–30.

46. Karhu, H.; Kalantar, A.; Väyrynen, I.J.; Salmi, T.; Murzin, D.Y. XPS analysis of chlorine residues in supported Pt and Pd catalysts with low metal loading. *Appl. Catal. B Environ.* **2003**, *247*, 283–294. [CrossRef]

47. Weng, X.; Shi, B.; Liu, A.; Sun, J.; Xiong, Y.; Wan, H.; Zheng, S.; Dong, L.; Chen, Y. Highly dispersed Pd/modified-Al$_2$O$_3$ catalyst on complete oxidation of toluene: Role of basic sites and mechanism insight. *Appl. Surf. Sci.* **2019**, *497*, 143747. [CrossRef]